The Effect of Quaternary Additions on the Oxidation Behavior of Hf-Doped NiAl

B. A. Pint, K. L. More and I. G. Wright
Oak Ridge National Laboratory
Oak Ridge, TN 37831-6156

Abstract

Cast model alloys, based on β-NiAl+0.05at%Hf, were used to study the effects on oxidation behavior of elements that are commonly present in low activity aluminide bond coatings on single-crystal, Ni-base superalloys. Single additions of Re, Ti, Ta and Cr were examined in cyclic and isothermal exposures at 1100-1200°C in order to determine their effect on the oxide growth rate and resistance to scale spallation. With 1at% additions, all of these elements were found to be detrimental to the oxidation performance of the base NiAl+Hf alloy. Additions of Re and Cr were found to form second phase precipitates in the alloy which appeared to lead to scale spallation, while additions of Ti and Ta were internally oxidized and incorporated into the scale as grain boundary segregants. These results suggest that it is necessary to minimize the levels of these types of elements that enter Hf-modified aluminide coatings by using process modifications or a diffusion barrier.

Keywords: NiAl, high temperature oxidation, reactive element effect, hafnium, bond coats

Introduction

Beta-phase nickel aluminide is commonly used as a model alloy to study high temperature oxidation behavior because it is a single phase alloy and a primary alumina former which forms no transient Ni-rich oxide[1-2]. Aluminide coatings, especially those with Pt, are one major class of coatings used on Ni-base superalloys to improve high temperature oxidation resistance[3-5]. When aluminide coatings are used as a bond coat beneath a ceramic thermal barrier coating (TBC), the adhesion of the alumina scale is of particular interest because spallation leads to loss of the ceramic layer. Previous work[6-9] has shown that the addition of ≈0.05at%Hf to β-NiAl results in the slowest-growing, most

adherent alumina scale observed on any alumina-former. It is considered to be an "ideal" alumina former. The addition of 0.05at%Hf reduces the alumina scale growth rate by a factor of 10 compared to undoped NiAl or (Ni,Pt)Al at 1100°-1200°C.[7] This has significant implications for the development of long-life, high temperature bond coats. If the alumina scale on a bond coating grows at a slower rate, strains associated with growth and cooling are nominally lower, and a longer exposure time is required to achieve critical scale thicknesses where spallation begins.

The benefit of Hf from the substrate entering an aluminide coating has been noted previously.[10] However, achieving a Hf dopant level in a commercial aluminide coating that achieves the excellent performance observed for a cast laboratory alloy is difficult. A primary problem is uniformly incorporating the optimum amount of Hf into the coating.[11] If the Hf content is too low, little or no benefit will be observed, whereas higher than optimum Hf levels will accelerate the scale growth by oxidizing internally and forming HfO_2 pegs which transport oxygen rapidly. Another significant issue is that fabrication of aluminide coatings by various aluminizing processes involves diffusion of superalloy substrate elements. For coating fabrication processes that have a low Al activity, there is an outward diffusion of substrate elements. While Ni is the primary diffusing species, other elements in the superalloy substrate also become incorporated[12] into the aluminide coating such as Cr, Ta, Ti, Mo and Re depending on the superalloy composition. Therefore, with current coating practices, the coating would not be solely Hf-doped NiAl but would also contain various other elements.

The effects of these additional elements on the oxidation behavior of NiAl has been studied to some degree but generally not in conjunction with a reactive element addition such as Hf. Chromium has been the most widely studied additive. The effect of Cr on the $\theta-\alpha$ phase transformation[13] has been considered along with the effect of high Cr concentrations on compositions with poor oxidation resistance.[14] However, compared to Zr- or Y-doping, Cr additions were not found to improve oxidation behavior of NiAl.[15-17] Compared to undoped NiAl, a 0.1at.% Mo addition was found to have no effect on adhesion or morphology of the alumina scale.[18] In various studies, Ta,[19] Ti,[20] and Re[14,21] have been reported to improve oxidation behavior. However, none of these elements possess the combination of ion size and oxygen/sulfur affinity typical of fully-effective reactive element dopants.[22-23] Results for Ta-

modified NiAl alloys showed less spallation than undoped NiAl[16] but, unless doped with Y, scale spallation and interfacial voids were observed similar to undoped NiAl.[24] Additions of Ti were found to be only marginally beneficial to the oxidation behavior of NiCrAl[25], Ni_3Al[26] and NiAl.[15] Incorporating Re into MCrAlY coatings was found to be beneficial,[21] but in general the oxidation resistance of MCrAlY alloys is inferior to NiAl because of a higher thermal expansion.[27-29] Adding 5at.%Re to β-NiAl resulted in no improvement in scale spallation resistance.[16] Incorporating Re into a two phase β-NiAl+α-Cr alloy reduced the metal recession rate, but the attack was significant even with Re.[14]

The objective of this study was to identify the combined effect of Hf and elements selected as representative of those likely to become incorporated into the coating and, particularly, into the alumina scale. Cast alloys were used in order to accurately control composition and isolate experimental variables. With a base of NiAl + 0.05at%Hf, castings were made with 1at% additions of Cr, Re, Ti or Ta. Chromium levels up to 10at% also were investigated because of its well-known beneficial effect on hot corrosion resistance,[30] experimental evidence that 3-5at% is found in coatings,[12] and more than 1at%Cr is necessary to confer hot corrosion resistance.[31,32] In general, all of the elements were detrimental to some degree to the outstanding oxidation performance of Hf-doped NiAl.

Experimental Procedure

All of the alloys were inductively melted and cast using a chilled copper mold and annealed for 4h at 1300°C in sealed quartz ampules. As-cast alloy compositions are given in Table I. Attempts were made to maintain 0.05at%Hf and 50at%Al as a base alloy in each case. However, since Cr is not soluble in the β phase at these compositions, the Al content in the Cr-containing alloys was reduced in order to maintain approximately 50at% Al in the β phase. In preliminary castings this adjustment was not made, and an extremely brittle material resulted. Coupons ≈15mm in diameter and 1.5mm thick were cut and polished to a 0.3μm finish. Cyclic oxidation experiments were conducted at 1100°-1200°C either (1) in an automated test rig where the specimens were hung by Pt-Rh wire in a flowing O_2 environment and cycled for 1h at temperature with 10min cooling between cycles or (2) in air in a box or tube furnace for 100h cycles with specimens in individual alumina crucibles which capture any spalled oxide.[33]

Oxidation kinetics were measured in isothermal experiments with dry flowing O_2 using a Cahn model 1000 microbalance.

After oxidation, specimens were characterized by electron microprobe (EPMA) and by field emission gun, scanning electron microscopy (SEM) and transmission electron microscopy (TEM); both equipped with energy dispersive x-ray (EDX) detectors for determining chemical compositions. Metallographic cross-sections were made by first Cu-plating prior to sectioning. TEM specimens were fabricated using focused ion beam milling (FIB).[34]

Results

Alloy Characterization

Figure 1 shows the microstructure of each of the alloys after polishing and etching. In Figure 1a, the grains are elongated several millimeters in the radial direction of the casting and vary in width, depending on location in the casting. This resulted in a slightly finer grain size in the center and a coarser grain size near the edge. Small particles in the casting possibly mark the as-cast grain structure prior to the 1300°C anneal or a subgrain structure. Each of the additions appeared to increase the number of precipitates in the alloy relative to the base Ni-50Al+0.05Hf alloy and to reduce the elongated nature of the grain structure to a large extent. Most of the doped castings had a columnar grain structure near the edge of the casting, but the center region consisted of equiaxed grains typical of Figures 1b-1h. Any segregation which may have occurred during solidification was likely minimized by the 4h anneal at 1300°C. The addition of 1%Re noticeably improved the quality of the casting by eliminating cracks and, based on specimen preparation, the casting was less brittle than the other materials. The addition of Ta appeared to result in numerous precipitates (Figure 1c) rich in Ni and Ta (by EPMA). With increasing Cr content, the grain size appeared to decrease and the Cr-rich, α phase precipitates increased in density and average size, Figures 1e-1h.

Oxidation Behavior at 1150°C

Figure 2a shows the specimen mass changes for the alloys in this study during 1h cycles at 1150°C. Two separate tests of the base alloy, NiAl+Hf, provide a reference for comparing the behavior

of the other alloys. The uniform dark gray surface oxide and the low specimen mass gain throughout the test reflected the formation of an adherent, slow-growing alumina scale. In contrast, undoped NiAl showed mass losses after the first 60 cycles, indicating scale spallation. Each of the alloys with additions initially showed higher mass gains than the base alloy. This reflects a more rapid rate of scale formation. Alloys with additions of 1Ta, 2Cr and 5Cr had the highest mass gains after 1000 cycles, a factor of 4 higher than the base alloy, indicating a fairly adherent but faster-growing alumina scale than that formed on the base alloy. The alloy with 1Ti also showed an adherent scale but exhibited a slightly lower mass gain. The mass change curves for the alloys containing 1Re and 10Cr showed mass losses at the end of the test and scale spallation was evident on these specimens. The specimen with a 1Cr addition produced the closest match to the results for the base alloy; little spallation was observed, but it did show a slightly higher mass gain. A summary of the mass changes after 1000h is given in Table II.

To put the performance of these alloys in context, some test data from related studies[18,35] of composition effects is included in Figure 2b. There has been speculation that the amount of Al in NiAl is critical to its oxidation performance.[36] This idea is primarily based on theoretical changes in the Ni and Al diffusion coefficients.[37] The alloys in the present study have varying amounts of Al, particularly the Cr-doped alloys, Table I. These results show little effect of varying the Al content within the β phase field. Undoped Ni-50at.%Al alloys, Ni-47.5at.%Al and Ni-52.5at.%Al performed similarly at 1150°C. With Hf doping, Al contents of 45at.%Al and 47.5at.%Al performed similarly to the base alloy. The specimen with 1Re and no Hf produced more spallation than undoped NiAl. The specimen with only an addition of 1Ta showed mass losses equal to undoped NiAl. Only the addition of 1Ti showed some improvement in performance, consistent with earlier work.[15] However, even this alloy showed significantly more scale spallation compared to any of the Hf-doped alloys in Figure 2a.

To confirm the faster scale growth rate suggested by the mass gain curves in Figure 2a, SEM examinations were performed and metallographic cross-sections were made of each specimen. After 1000 cycles, the scales first were examined in plan-view by SEM. Figure 3a shows the typical ridge structure observed for RE-doped NiAl.[1,8,9,28,38] The tiny bright particles on each ridge are likely HfO_2 particles which nucleate and grow during extended exposures at high temperature as a result of the

outward diffusion of Hf along the scale grain boundaries.[22,39] Despite being exposed to 1000 cycles, the scale showed few defects (e.g. cracks, spalled regions) except at the edge of the specimen where scale spallation did occur. The specimens with additions of 1Re and 10Cr showed obvious signs of spallation. For the specimen with Ti, a large number of particles were observed at the scale surface, Figure 3b, and the Ti signal was strongly observed in EDX analysis suggesting that a large amount of Ti was present in the scale or in the particles at the scale surface. Because of their small size and a lack of difference in atomic number, it was difficult to identify Ti-rich particles. On the specimen containing 1Cr (Figure 3c) and higher levels of Cr, the ridge spacing appeared finer than on the base alloy indicating a smaller Al_2O_3 grain size. However, ridge spacing also varies with substrate orientation;[1,40,41] therefore, this observation does not conclusively demonstrate that Cr additions reduce the alumina grain size.

To provide information on the scale thickness, metallographic cross-sections were made. Figure 4a shows a metallographic cross-section from the base alloy NiAl+Hf after 1000, 1h cycles at 1150°C. The scale was thin but not uniform in thickness. The white arrow in 4a marks a metal intrusion into the scale, as was observed after 100h at 1100°C in a previous study.[9] Figure 4b shows an area where the oxide on the Re-containing alloy had spalled. With additions of Ta and Ti (Figures 4c and 4d, respectively), a thicker alumina scale was formed and there are second phase oxides present in the scale indicating that large amounts of both elements were incorporated in the scale. The oxide protrusions at the metal-oxide interface indicate that internal oxidation of these elements also occurred which would increase the specimen mass gain. In the case of the 1Ta addition, Ta-rich precipitates (arrows in Figure 4c) were identified in the metal and in the oxide using EPMA. The scales on the Ta- and Ti-containing specimens appeared similar in thickness despite the larger mass gain for the Ta-containing specimen, Figure 2a. The mass gain difference appeared to be the result of heavy internal oxidation due to a casting defect in the NiAl-1Ta+Hf specimen and was not observed in subsequent tests.

Figures 4e-4h show substrates with increasing Cr contents and respective increases in the number of α-Cr precipitates (lighter particles) in the substrate. These precipitates were frequently observed at the metal-scale interface, particularly with 10Cr (arrow in Figure 4h). With the addition of only 1Cr, the scale thickness was only slightly thicker than on the base alloy, consistent with the mass change, Figure

2a. The addition of 2-10%Cr appeared to increase the scale thickness to a similar degree as the additions of Ta and Ti.

Oxidation Behavior at 1100°C

At a lower test temperature, similar results were observed during 1h cycles, Figure 5. In this case, alloys with additions of 1Ti, 1Ta, 2Cr and 5Cr all showed increased mass gains of 2-3X after 1000 cycles compared to the base alloy. The alloy with 10Cr showed a 4X increase in mass gain after 1000h which was similar to that observed for a cast NiAl-5at.%(20wt.%)Pt alloy. The addition of Pt improves the alumina scale adhesion on undoped NiAl but does not change the scale growth rate.[7,35] The lower mass gain for the specimen with 1Re was again attributed to observed scale spallation. The addition of 1Cr resulted in an ≈50% increase in mass gain. The final specimen mass gains after 1000, 1h cycles also are given in Table II.

To complement the data from 1h cycles, 100h cyclic tests also were conducted at 1100°C. Because these tests were contained in alumina crucibles, it was possible to quantify the spallation behavior of the various alloys as the difference between the total and specimen mass changes.[33] Figure 6 indicates the performance of the various aluminides; solid lines show the total mass gains and dashed lines show the specimen mass changes. The data from this test are summarized in Table III for clarity. The total and specimen mass gains after 20, 100h cycles are listed as well as the specimen mass gains after 1000h (10 cycles) for comparison to the final specimen mass gains after 1000, 1h cycles at 1100°C, Table II.

The range of behavior in 100h cycles was bounded by undoped NiAl, which had the highest total mass gain and a large deviation between total and specimen mass changes, and the base alloy, NiAl+Hf, which had the lowest total mass gain and an ≈10% difference (0.09-0.12mg/cm^2) between the specimen and total mass gain in two separate tests. The addition of 1Cr resulted in increased total mass gain but little spallation, Table III. However, higher Cr levels all caused higher mass gains and increased levels of spallation. The alloy with 2Cr appeared to have an anomalously high mass gain and spallation that was not found in the other tests in the study. The most spallation of any of the Hf-doped alloys was

observed for 10Cr. Additions of Ta and Ti also increased the total mass gain but resulted in little scale spallation. For the specimen with Re, the mass change in this test more clearly demonstrated that the addition of Re caused both an increase in the scale growth rate and also a significant amount of scale spallation. This was harder to discern from the specimen mass change in 1h cycles. However, the increase in total mass gain due to the addition of Re was not as high as that for some of the other additions. This likely reflects that the more noble Re addition was not being internally oxidized which would have added to the mass gain.

Cross-sections of the specimens after the twenty 100h cycles are shown in Figure 7. Compared to the cross-sections after exposure at 1150°C, the base NiAl+Hf alloy showed a more uniform scale thickness but also more oxide penetrations, Figure 7a. In this image and some others, the scale has separated from the Cu-plating resulting in a thin layer of epoxy in the image. In general, specimens with additions of 1Ta and 1Cr (Figures 7c and 7e respectively) did not show significantly thicker scales but did have more oxide penetrations. However, with increasing Cr contents, there was a clear increase in the scale thickness, Figures 7f-7h. The specimen containing Ti had both a thicker scale and more oxide penetrations than the base alloy. This explains its higher mass gain in Figure 6. The cross-section of the Re-doped specimen confirmed the formation of a thicker scale and spallation, Figure 7b.

Oxidation Behavior at 1200°C

While bond coats on superalloys are less likely to be used at temperatures as high as 1200°C, increasing the temperature exaggerated and confirmed some of the observations at lower temperatures. It also demonstrated that the exceptional oxidation behavior associated with Hf-doping is observed even for thicker scales, although a 1000h exposure at 1200°C begins to show some potential problems with the base alloy. For the quaternary additions, the same general trends continued in both 1h and 100h cyclic tests at 1200°C

Figure 8 shows the performance of the alloy set in 1h cycles. The base NiAl+Hf alloy showed clear spallation in this test. However, another alloy with similar composition (marked NiAl+Hf, low C) showed very little spallation after 1000h. In this test, the effects of Ti and Ta appeared to be less pronounced with only slightly higher mass gains than the base alloys and little evidence of scale

spallation. The addition of Re clearly showed a negative effect with a mass loss after 1000 cycles. The mass gain of NiAl-1Cr+Hf was higher than the base alloy but lower than the low C version of the base alloy, suggesting only a low level of spallation at this temperature. However, increases in mass gains and scale spallation were noted with higher levels of Cr. Because of the competing processes of faster scale growth and scale spallation, it is difficult to rank the performance of these materials based only on specimen mass changes. It appeared that with additions up to 5Cr, scale adhesion was not strongly affected. However, with an addition of 10Cr, a significant mass loss (-24.1mg/cm^2) was observed after 1000 cycles.

Cyclic testing with 100h cycles showed similar results, Figure 9. In this case, the specimen mass curves were not included but the final specimen mass changes are listed in Table III. The specimens with the highest total mass gains showed large amounts of scale spallation, with undoped NiAl showing almost 100% scale spallation after each cycle. The best behavior was observed for the base alloys. As with 1h cycles, the low C version of NiAl+Hf showed less spallation (a remarkably low 0.01mg/cm^2 compared to the base alloy of 1.52mg/cm^2) but surprisingly both alloys had similar total mass gains. Additions of 1Cr, Ti and Ta showed slightly higher total mass gains than the base alloy but the specimen with a 1Cr addition had the most spallation of the three based on the much larger difference between the total and specimen masses, Table III. Increasing Cr levels showed increasing total mass gains and amounts of spallation. The alloy with 1Re also showed a large amount of spallation.

Cross-sections of the reaction products after 10, 100h cycles also were examined. However, because most of the specimens had some degree of scale spallation, less comparative information was obtained from these scale cross-sections. Therefore, Figure 10 shows scale cross-sections after an isothermal 100h exposure at 1200°C. After just one cycle, it is clear that each of the additions resulted in a thicker oxide compared to the base alloy. The scale on the base alloy (Figure 10a) again showed metal protrusions as was observed at 1150°C. The specimen containing Re showed a thicker oxide as well as scale spallation, Figure 10b. As expected from the cyclic data, additions of Ta, Ti and 1Cr slightly increased the scale thickness, Figures 10c-10e. With increasing levels of Cr, the scale increased in thickness, Figures 10e-10h. The specimen with 10Cr also showed a large degree of scale spallation.

In order to confirm the dopant effects on the scale growth rate at 1200°C, two isothermal runs of 50 and 100h were made at 1200°C for each alloy and the oxidation kinetics were measured continuously using a microbalance. Table IV lists the parabolic rate constants measured for each alloy. As has been reported previously,[7-8] the parabolic rate constant for undoped NiAl is an order of magnitude higher than for NiAl+Hf. The rate constants for the quaternary additions are generally 2-5X higher than the base alloy. More scatter was observed for the Cr containing alloys than for the other additions. To quantify the observations made at longer times in the cyclic tests and to minimize the transient effects, the total mass gains in Figure 9 were plotted versus the square root of time[42] and an effective parabolic rate constant was calculated. For those alloys with large amounts of scale spallation, higher rate constants reflect scale loss and re-growth and a parabolic relationship was not actually followed. However, for the alloys with low amounts of scale spallation, i.e. those with additions of Ta, Ti and 1Cr, the results were informative. The rate for the specimen containing Ti was almost identical to the base alloy, Table IV. Additions of Ta and 1Cr increased the rate by a factor of 2. Compared to the base alloy, the low C NiAl+Hf had the lowest rate constant of all, reflecting its exceptional scale adhesion after 1000h.

A similar comparison was made for isothermal results and a parabolic fit of the total mass gain data at 1100°C, Table IV. Compared to 1200°C, the rates are up to an order of magnitude slower but similar trends continued. For most of the quaternary additions, the isothermal rates at 1100°C were significantly higher than the base alloy, reflecting more transient effects at the lower temperature. As at 1200°C, the effective rates were mainly lower during the 2000h cyclic test. However, in this case, the rates for the lowest impact quaternary additions were at least 2-3X higher than the base alloy. The comparisons in Table IV suggest that the impact of quaternary additions was reduced at higher temperatures like 1200°C but were more pronounced at lower temperatures where bond coats operate in practice.

TEM Analysis

Since thinner scales are more amenable to TEM analysis, oxides were examined after 2h at 1200°C. Figures 11-13 show representative areas of the scales. The scale on the base alloy showed the typical α-Al_2O_3 scale found on RE-doped NiAl, Figure 11. At longer oxidation times, these grains will

elongate to form a columnar grain structure.[7-8,43] Ridges, which are remnants of the θ−α phase transformation,[1,38,41] were observed above each grain boundary. Away from the scale grain boundary, the scale was much thinner, reflecting that the growth of the scale was primarily by diffusion along these short-circuit paths. Where there were no grain boundaries, the scale grew more slowly. For new oxide to form at the metal-oxide interface at the center of an oxide grain, oxygen would have to diffuse along the metal-oxide interface from a scale grain boundary. In this specimen and in each of the others, Hf ions were found to segregate to the scale grain boundaries using microchemical (EDX) analysis. Thus, none of the dopants prevented Hf from segregating to the scale grain boundaries.

Additions of Ta and Ti showed little effect on the scale microstructure (Figures 12a and 12b) but small amounts of Ta and Ti ions were detected on the oxide grain boundaries. Unfortunately, no oxide protrusions or second phase oxides were observed in the TEM thin sections. With Re and 2Cr additions, second phase α particles were observed, Figures 12c and 13. For the specimen containing Re, the precipitates were large and clearly observed in both the metal and oxide, indicating low solubility for Re in the β phase. Voids also were present in the scale and the oxide had a much different structure than on the other alloys. In plan view, Figure 14b, the scale appeared significantly different than the base alloy (Figure 14a) or any of the other alloys (e.g. Figure 14c). After longer exposures, it was not surprising that the oxide spalled more readily from this alloy (see Figures 8, 9 and 10b). After 1000h at 1200°C, these α-Re precipitates continued to grow and can be clearly seen in a EPMA back-scattered electron image, Figure 15. On the alloy grain boundaries and at the alloy-scale interface, the particles were mostly spherical while within the grains some of the particles were needle-like.

Only one Cr-containing alloy was analyzed by TEM, NiAl-2Cr+Hf, Figure 13. On first look, the oxide appeared similar to that on the base alloy, although the grain size was much smaller. However, an EDX map of the boxed area in Figure 13a showed small α-Cr particles at the alloy-scale interface, Figure 13b. These particles were much smaller than the α-Re particles. Based on the scale cross-sections, it is likely that with longer exposures or higher Cr contents larger precipitates would form, possibly degrading scale adhesion.

Discussion

In searching for improved aluminide coating performance, one of the most promising strategies is to replace or supplement Pt with Hf. The addition of Hf has the possibility of not only improving scale adhesion but also reducing the scale growth rate.[6-9] The purpose of this study was to consider what effect other dopants, likely to be present in a diffusion aluminide coating, would have on the performance of Hf-doped NiAl. At concentrations ≥1at.%, all of these additions appeared to have negative effects. However, most of these elements, except Cr, will be present at lower levels in the coating.[12] Thus, they may have a relatively minor negative effect on the performance of a Hf-modified aluminide coating. The important point is that processing strategies which limit the amount of these elements in the coating are likely to improve the oxidation performance of the coating.[28]

In explaining the negative effect of these quaternary additions, it is necessary to first consider why the addition of Hf provides such an extreme benefit. Hafnium appears to act like other reactive element additions in that it segregates to the alumina grain boundaries and diffuses outward during oxidation, nucleating HfO_2 particles at the scale-gas interface.[8,22,23,28,39] Compared to Y, Hf has the benefit of being more soluble in NiAl so the formation of Hf-rich precipitates is minimized with a 0.05% dopant level. The formation of NiY_x precipitates and their subsequent internal oxidation has been linked to increased amounts of scale spallation.[27,44] A more soluble dopant like Hf should have an advantage over Y. But this does not explain the additional benefit of Hf compared to Zr, which appears to have a similar solubility level.[8] Oxidation rates for NiAl+Zr were found to be 2-4X higher than NiAl+Hf.[8] Both dopants are predicted to have similar ionic radii, charge and oxygen affinity so it is not clear why Hf performs so much better. If one assumes that Hf has a higher "effective" ionic radius because of its much higher atomic number, it could be argued that the larger Hf segregant ion could be less mobile and more effectively disrupt boundary diffusion of Al (and possibly O) when segregated to the α-Al_2O_3 grain boundaries. However, there is no experimental basis for making such an assumption. The additional benefit of Hf also could be a result of a larger Al_2O_3 grain size. However, there is no obvious reason why a larger grain size should occur with Hf doping and not with Zr doping. Rather than due to grain

growth, larger scale grains on NiAl would likely come from differences in the nucleation of α grains from the transient cubic alumina phases.[1,38,41] Large dopant ions have been found to inhibit the θ- to α-Al_2O_3 phase transformation,[38,45] but again, unless it is assumed that there is an effective ionic size difference between Zr and Hf, both ions should have similar effects on the phase transformation and thus the scale grain size. Thus, at present there is no certain explanation for the additional benefit of Hf compared to Zr.

In general, the maximum benefit for Hf is observed in NiAl and Fe-Al materials.[46,47] Hafnium additions are not as effective as Y in FeCrAl[47] and NiCrAl[48,49] in improving scale adhesion. This observation may be further indication of a negative Cr-Hf interaction. The effectiveness of Hf also may be related to indigenous sulfur in the castings. Chromium is the major source of S in these castings, Table I. Glow discharge mass spectrometry analysis of NiAl cast at ORNL showed less than 1.4ppma (1 ppmw) S.[50] The addition of Cr raised the S level to 4-8 ppma, Table I. In ORNL MCrAl castings, the S level can be 20-30ppma.[27,47] The addition of S may inhibit the beneficial role of Hf, particularly because the Hf content is so low. It also has been suggested that Hf is not as effective in countering the detrimental role of S as Y.[51] However, S levels are nearly identical in Fe_3Al and FeCrAl (20-30ppma) and Hf-doped Fe_3Al shows better scale adhesion and a lower scale growth rate than FeCrAl+0.05at.%Hf.[47]

The results at 1200°C illustrate the influence of a second important impurity element, carbon. The Hf/C atomic ratio or the ratio of Hf to the combined C, N and O levels, has been useful in interpreting the performance of NiAl and both model and commercial Ni-base superalloys.[49] Carbon is likely a more important factor with Hf because HfC is more stable than other reactive element carbides,[51] particularly Y. Hydrogen de-sulfurizing[52] has been shown to reduce both the C and S levels in commercial second generation Ni-base superalloys,[53,54] suggesting that the treatment may be beneficial because it removes S but also because it activates the 0.05at% Hf addition by removing the C. The role of C in NiAl+Hf is still being investigated but, at 1200°C, it is clear that a low C version showed improved scale spallation resistance (Figures 8 and 9 and Tables II-IV). For this study of quaternary alloy additions to NiAl+Hf, the C levels were constant (Table I) and not thought to alter the scale growth rate or be as important a

factor at 1100°-1150°C.

Additions of Ta or Ti to NiAl+Hf, which are more oxygen-active elements than Cr or Re, were found both as second phase particles and as ions segregated to the α-Al_2O_3 scale grain boundaries. Tantalum has the low oxygen potential necessary for internal oxidation thus increasing the oxidation rate. Titanium was observed to become strongly incorporated into the scale (Figure 3b), likely by diffusion from the alloy into the scale, rather than internal oxidation. When Ta- or Ti-rich oxide particles become incorporated into the scale, the scale growth rate is accelerated since these particles provide a fast diffusion path either through the oxide particle or at the particle interface, thus negating one of the principal benefits of Hf doping. Alloy precipitates rich in Ta were evident in each case, Figures 1c, 4c, 7c and 10c. No alloy Ti-rich precipitates were observed by light microscopy or EPMA in this study but comparisons of the alumina scale morphology on NiAl with alloy additions of Ti compared to TiO_2-dispersed NiAl suggested that the Ti is not uniformly present in NiAl.[8,38] If the increased scale growth rates were related only to internal oxidation of second phase particles, then the negative effect of these elements should be diminished if they are present at lower levels.

Using TEM/EDX, Ta and Ti ions were found to segregate to the grain boundaries along with Hf. This behavior is not surprising as both Ta and Ti were found to segregate to the grain boundaries of α-Al_2O_3 formed on FeCrAl when they were added to the alloy as oxide dispersions at a 0.2cation% level.[23] However, as individual dopant oxide additions to FeCrAl, they did not perform as well as other reactive elements such as Y and La, similar to observations for NiAl, Figure 2b The previous study on FeCrAl concluded that Ta and Ti did not have a sufficiently large ion size to produce all of the reactive element effects. Yet in this case, if the presence of Ti or Ta ions on the α-Al_2O_3 grain boundaries disrupts the effect of Hf, then even small concentrations in the coating could be detrimental.

In the case of Cr and Re additions, a different detrimental effect was observed. Instead of being incorporated into the scale as segregants and oxides, these elements appeared to cause the formation of α-Cr or α-Re precipitates at or near the metal-scale interface. Similar precipitates containing Cr, Re and/or Mo have been observed in aluminide coatings.[55,56] These particles are believed to disrupt the metal-oxide adhesion causing increased scale spallation.[9] However, both additions did appear to

accelerate the rate of scale growth. It is not clear how this occurred. In the case of Cr, additions to NiAl have been reported to accelerate the θ- to α-Al_2O_3 phase transformation.[13,57] Possibly this occurs by increasing the number of α nuclei. This mechanism also would result in a finer α-Al_2O_3 grain size. By increasing the number of grain boundaries, which have been shown to be the only viable diffusion pathway in α-Al_2O_3,[58] the scale growth rate should be increased.[59] However, it is difficult to draw conclusions about the effect of Cr (or the other dopants) on the scale grain size because the grain size can be affected by the NiAl substrate orientation.[1] For these polycrystalline specimens, a statistical analysis would be necessary to prove a finer scale grain size on a doped substrate relative to the base alloy.

The addition of Re appeared to affect both scale adhesion and the growth rate. As mentioned previously, one difficulty in interpreting mass gain data is the combined effect of spallation and accelerated scale growth rates. Mass loss from scale spallation can counter some of the increased mass gain due to a faster scale growth rate. However, the isothermal results at 1200°C clearly show an increase in the scale growth rate with the addition of Re, Table IV. As mentioned above for Cr additions, this could have been due to a finer scale grain size, Figure 12c. But Re also appeared to change the columnar grain structure and the ridge structure of the scale, Figure 14b. Rhenium ions were not detected as segregants to the α-Al_2O_3 grain boundaries. This is similar to the behavior of Mn and V in FeCrAl;[23] neither were detected as segregants in the alumina scales.[23] The reason proposed for that behavior was low oxygen affinity, an explanation that also could apply to Re. The Re particles observed in the scale (Figure 12c) could have resulted from incorporation by the inward growing scale.

One source of error in this work was the casting quality of the substrates. Because NiAl is a brittle material, it can have cracks or other defects in the casting which will alter the mass gains. The cross-sectional specimens were made to verify the mass gain data. Examples of abnormally high mass gains caused by casting defects were NiAl-1Ta+Hf at 1150°C (Figure 2a) and NiAl-2Cr+Hf in 100h cycles at 1100°C (Figure 6). However, these defects were not a dominant aspect. The addition of Re noticeably improved casting quality but also caused scale spallation.

These results indicate that while Hf doping is a promising strategy for improving bond coat performance, there may be limitations to its effectiveness that need to be taken into account during

processing. Strategies that reduce impurities in the coating may improve performance but also may increase susceptibility to hot corrosion attack if the Cr content is too low.[28,32] This type of information is necessary in assessing the potential benefit of incorporating Hf into a cost-effective, commercial bond coating and determining composition guidelines for maximizing its benefit. More work will be necessary to clearly define the limitations of this strategy and perhaps suggest a mechanism for the amazing effect of Hf doping.

Summary

Additions of Cr, Re, Ti and Ta to NiAl+Hf were all found to have negative effects on the oxidation performance at 1100-1200°C compared to the Hf-doped NiAl base alloy. In each case, the addition of another element with Hf accelerated the scale growth rate. With the addition of Re or Cr, second phase α precipitates formed and these appeared to lead to increased scale spallation, as well as to faster scale growth rates. With increasing Cr levels up to 10at%, the negative effects on scale growth rate and spallation increased. Additions of 1at% Ta or Ti were found to internally oxidize and these elements also become incorporated into the alumina scale as grain boundary segregants and oxide particles. These results indicate that for an aluminide coating to have the maximum Hf benefit on scale adhesion and a reduced scale growth rate, the concentration of other elements that are typically present in the coating should be kept to a minimum.

Acknowledgments

The authors would like to thank G. Garner, L. D. Chitwood, L. Walker and K. S. Trent for assistance with the experimental work. P. F. Tortorelli, J. R. DiStefano and J. A. Haynes provided helpful comments on the manuscript. This research was sponsored by the U.S. Department of Energy, Advanced Turbine Systems program under contract DE-AC05-00OR22725 with UT-Battelle, LLC.

References

1. J. Doychak, in *Intermetallic Compounds, Vol.1: Principles*, J. H. Westbrook and R. L. Fleischer eds. (John Wiley & Sons, New York, NY 1994) p.977-1016.
2. M. P. Brady, B. A. Pint, P. F. Tortorelli, I. G. Wright, and R. J. Hanrahan, in *Materials Science and Technology: A Comprehensive Treatment*, Vol.19B, Corrosion and Environmental Degradation of Materials, (Wiley-VCH, Weinheim, Germany, 1999) p.229-325.
3. G. Lehnert and H. Meinhardt, *Electrodepositoin and Surface Treatment*, **1**, 189-97 (1972-1973).
4. M. S. Farrell, D. H. Boone and R. Streiff, *Surface Coatings and Technology*, **32**, 69-84 (1987).
5. B. M. Warnes and D.C. Punola, *Surface and Coating Technology,* **94-95**, 1-6 (1997).
6. J. Doychak and B. A. Pint, manuscript in progress.
7. B.A. Pint, I. G., Wright, W. Y. Lee, Y, Zhang, K. Prüßner and K. B. Alexander, *Materials Science and Engineering*, **A245**, 201-211 (1998).
8. B. A. Pint, *Oxidation of Metals* **49**, 531-60 (1998).
9. B. A. Pint, K. L. More, I. G. Wright and P. F. Tortorelli, *Mater. High Temp.* **17**, 165-71 (2000).
10. R. Streiff and J. M. N'Gandu Muamba, *Journal of Metals*, **40**(11) 104 (1988).
11. G. Y. Kim, L. M. He, J. D. Meyer, A. Quintero, J. A. Haynes and W. Lee, submitted to *Metallurgical and Materials Transactions* (2001).
12. Y. Zhang, W. Y. Lee, J. A. Haynes, I. G. Wright, B. A. Pint, K. M. Cooley and P. K. Liaw, *Metallurgical Transactions A*, **30A**, 2679-87 (1999).
13. M. W. Brumm and H. J. Grabke, *Corrosion Science* **33**, 1677-90 (1992).
14. M. A. Phillips and B, Gleeson, *Oxidation of Metals* **50**, 399-429 (1998).
15. C. A. Barrett,*Oxidation of Metals* **30**, 361-90 (1988).
16. C. A. Barrett and R. H. Titran, NASA Report TM-105620, Lewis Research Center, Cleveland , OH (1992).
17. J. G. Smeggil, *Surface Coatings and Technology,* **46**, 143-53 (1991).
18. B. A. Pint, unpublished research, Oak Ridge National Laboratory, Oak Ridge, TN (1997).
19. J. M. N'Gandu Muamba and R. Streiff, *Materials Science and Engineering* **A121**, 391-405 (1989)
20. G. H. Meier, F. S. Pettit and J. L. Smialek, *Werkstoffe und Korrosion* **46**, 232-40 (1995).
21. W. J. Quadakkers, W. Stamm, N. Czech, E. Wallura, H. Hoven, F. Schubert,in Proceedings of Euromat '97, (IOM, London, 1997) pp.388-42
22. B. A. Pint, *Oxidation of Metals* **45**, 1-37 (1996).
23. B. A. Pint and K. B. Alexander, *Journal of the Electrochemical Society* **145**, 1819-29 (1998).

24. C. S. Giggins, B. H. Kear, F. S. Pettit and J. K. Tien, *Metallurgical Transactions* **5**, 1685-8 (1974).
25. D. Clemens, V. Vosberg, H. J. Penkalla, U. Breuer, W. J. Quadakkers and H. Nickel, *Fresnius Journal of Analytical Chemistry* **358**, 122-6 (1997).
26. S. Taniguchi and T. Shibata, *Oxidation of Metals* **25**, 201-16 (1986).
27. B. A. Pint and I. G. Wright, in *High Temperature Corrosion and Materials Chemistry*, Proc. v.98-9, P. Y. Hou, M. J. McNallan, R. Oltra, E. J. Opila and D. A. Shores, eds. (Electrochem. Soc., Pennington, NJ, 1998) pp.263-74.
28. B. A. Pint, J. A. Haynes, K. L. More, I. G. Wright and C. Leyens, in *Superalloys 2000*, T. M. Pollock, R. D. Kissinger, R. R. Bowman, K. A. Green, M. McLean, S. Olson and J. J. Shirra eds., (TMS, Warrendale, PA, 2000) p.629-38.
29. J. A. Haynes, W. D. Porter, B. A. Pint and I. G. Wright, submitted to *Materials at High Temperature*, 2002.
30. R. A. Rapp, *Materials Science and Engineering* **87**, 319-27 (1987).
31. C. Leyens, B. A. Pint and I. G.Wright, (2000) NACE Paper 00-260, Houston, TX, presented at NACE Corrosion 2000, Orlando, FL, March 2000.
32. C. Leyens, B. A. Pint and I. G.Wright, *Surface and Coatings Technology* **133-134**, 15-22 (2000).
33. B. A. Pint, I. G. Wright and P. F. Tortorelli, *Oxidation of Metals* **58**, 73-101 (2002).
34. K. L. More, D. W. Coffey, B. A. Pint, K. S. Trent, and P. F. Tortorelli, in Proceedings: Microscopy & Microanalysis 2000, Vol.6, Supp.2, G.W. Bailey, et al., eds., (Springer-Verlag, NY, 2000) pp. 540-1.
35. B. A. Pint, K. L. More and I. G. Wright, for submission to *Oxidation of Metals.*.
36. M. W. Brumm and H. J. Grabke, *Corrosion Science* **34**, 547-61 (1993).
37. S. Shankar and L. L. Seigle, *Metallurgical Transactions* **9A**, 1467-76 (1978).
38. B. A. Pint, M. Treska and L. W. Hobbs, *Oxidation of Metals* **47**, 1-20 (1997).
39. B. A. Pint, A. J. Garratt-Reed and L. W. Hobbs, *Journal of the American Ceramic Society* **81**, 305-14 (1998).
40. T. Homma, H. M. Hindam, Y. Pyun, W. W. Smeltzer, *Oxidation of Metals* **17**, 223-33 (1982).
41. J. Doychak, J. L. Smialek and T. E. Mitchell, *Metallurgical Transactions* **20A**, 499-518 (1989).
42. B. Pieraggi, *Oxidation of Metals* **27**, 177-85 (1987).
43. R. Prescott, D. F. Mitchell, M. J. Graham and J. Doychak, *Corrosion Science* **37**, 1341-64 (1995).
44. J. D. Kuenzly and D. L. Douglass, *Oxidation of Metals* **8**, 139-178 (1974).
45. P. Burtin, J. P. Brunelle and M. Soustelle, *Applied Catalysis* **34**, 225-38 (1987).

46. B. A. Pint, K. L. More, P. F. Tortorelli, W. D. Porter and I. G. Wright, *Materials Science Forum*, **369-372**, 411-8 (2001).
47. B. A. Pint, I. G. Wright and P. F. Tortorelli, for submission as ORNL report.
48. A. S. Khanna, C. Wasserfuhr, W. J. Quadakkers, and H. Nickel, *Materials Science and Engineering* **A121**, 185-91 (1989).
49. I. G. Wright and B. A. Pint, in Proc. SF2M 2000: Journées d'automne, (Société Française de Métallurgie et de Matériaux, Paris 2000), p. 86.
50. P. Y. Hou, private communication, 2001.
51. D. R. Sigler, *Oxidation of Metals* **32**, 337-55 (1989).
52. J. L. Smialek, D. T. Jayne, J. C. Schaeffer and W. H. Murphy, *Thin Solid Films* **253**, 285-92 (1994).
53. I. G. Wright, B. A. Pint, W. Y. Lee, K. B. Alexander and K. Prüßner, in *High Temperature Surface Engineering*, J. Nicholls and D. Rickerby, eds. (Institute of Materials, London, UK, 2000) p.95-113.
54. J. L. Smialek and B. A. Pint, *Materials Science Forum* **369-372**, 459-66 (2001).
55. H. M. Tawancy, N. M. Abbas, T. N. Rhys-Jones, *Surface Coatings and Technology*, **49**, 1-7 (1991).
56. J. A. Haynes, K. L. More, B. A. Pint, I. G. Wright, K. Cooley and Y. Zhang, *Materials Science Forum* **369-372**, 679-86 (2001).
57. R. Klumpes, C. H. M. Marée, E. Schramm and J. H. W. DeWit, *Materials and Corrosion* **47**, 619-24 (1996).
58. B. A. Pint, J. R. Martin and L. W. Hobbs, *Oxidation of Metals* **39**, 167-95 (1993).
59. C. Wagner, in *Atom Movements*, (Amer. Soc. Metals, Cleveland, OH, 1951) pp.153-73.

Table I. Chemical compositions of the cast alloys in atomic percent determined by induction coupled plasma analysis and combustion analysis.

	Ni	Al	Hf	Cr	Ta	Ti	Re	C	S(ppm)
NiAl	49.9	50.1	<0.01	<0.01		<0.01		0.04	<4
NiAl+Hf	49.8	50.1	0.05	0.01		<0.01		0.04	<4
NiAl+Hf(low C)	51.6	48.3	0.06	<0.01		<0.01		0.03	<4
1Re+Hf	48.4	50.5	0.04	<0.01	<0.01	<0.01	1.00	0.04	1
1Ta+Hf	48.7	50.2	0.05	<0.01	0.92	<0.01	<0.01	0.04	4
1Ti+Hf	48.6	50.3	0.05	<0.01	<0.01	1.00	<0.01	0.04	1
1Cr+Hf	50.1	48.8	0.05	0.98		<0.01		0.04	<4
2Cr+Hf	48.3	49.6	0.05	2.0		<0.01		0.04	4
5Cr+Hf	47.8	47.2	0.05	5.0		<0.01		0.04	8
10Cr+Hf	45.1	45.1	0.05	9.7		<0.01		0.04	5

Table II. Specimen mass changes (mg/cm^2) after 1000, 1h cycles at 1100°-1200°C.

	1100°C	1150°C	1200°C
NiAl	-0.52	-5.58	-15.64
NiAl+Hf	0.42	0.75	0.87
NiAl+Hf (low C)	0.45	0.79	1.87
NiAl-1Re+Hf	0.66	0.76	-0.74
NiAl-1Ta+Hf	1.10	2.24	2.55
NiAl-1Ti+Hf	1.10	1.46	2.26
NiAl-1Cr+Hf	0.66	1.01	1.54
NiAl-2Cr+Hf	0.95	2.20	1.56
NiAl-5Cr+Hf	1.17	2.14	2.87
NiAl-10Cr+Hf	1.57	1.06	-24.13

Table III. Mass changes after 100h cycles at 1100°C and 1200°C. The difference between the total and specimen mass gains is the amount of spalled oxide.

	20, 100h cycles at 1100°C		10, 100h at 1100°C	10, 100h cycles at 1200°C	
	Total	Specimen	Specimen	Total	Specimen
Alloy:	mg/cm^2	mg/cm^2	mg/cm^2	mg/cm^2	mg/cm^2
NiAl	4.81	-2.79	1.19	11.77	-12.36
NiAl+Hf	0.85	0.76	0.56	1.94	0.42
	0.86	0.74	0.49		
NiAl+Hf (low C)	0.76	0.78	0.55	1.75	1.74
NiAl-1Re+Hf	1.40	0.77	0.79	5.68	-5.39
NiAl-1Ta+Hf	1.61	1.56	1.16	2.83	2.38
NiAl-1Ti+Hf	1.88	1.87	1.57	2.54	2.17
NiAl-1Cr+Hf	1.21	1.14	0.82	2.27	1.06
NiAl-2Cr+Hf	2.47	2.03	1.54	4.27	-0.80
NiAl-5Cr+Hf	2.03	1.87	1.45	7.47	-1.96
NiAl-10Cr+Hf	1.98	0.72	1.17	11.36	-9.06

Table IV. Parabolic rate constants from thermogravimetry after 50-200h at 1100° and 1200°C and by fitting the 100h cycle total mass gain data at 1100°C and 1200°C.

	1200°C k_p (g^2/cm^4s) measured by TGA 50-100h	1200°C k_p (g^2/cm^4s) data fit for 100h cycles 1000h	1100°C k_p (g^2/cm^4s) measured by TGA 100h	1100°C k_p (g^2/cm^4s) data fit for 100h cycles 2000h
NiAl	9-13 x10^{-12}	82 x10^{-12}	36 x10^{-13}	39 x10^{-13}
NiAl+Hf	0.76-1.0	0.76	1.6	0.74-0.89
NiAl+Hf (low C)	0.79-1.0	0.56		0.83-1.0
NiAl-1Re+Hf	1.0-2.1	16	7.8	3.2
NiAl-1Ta+Hf	1.7-3.3	1.5	14	2.9
NiAl-1Ti+Hf	2.2-3.2	0.80	8.9	3.1
NiAl-1Cr+Hf	1.2-5.9	1.3	7.2	1.9
NiAl-2Cr+Hf	3.5-3.7	3.4	2.5	7.9
NiAl-5Cr+Hf	3.3-3.8	17	11	4.3
NiAl-10Cr+Hf	2.8-6.2	67	14	5.4

List of Figures

Figure 13. (a) TEM bright field image of the alumina scale formed on Ni-49Al-2Cr+Hf after 2h at 1200°C; (b) Cr EDS X-ray map at the interface reveals Cr-rich precipitates (arrows) in the metal adjacent to the metal-scale interface.

Figure 14. SEM plan view images of the surface scale after 2h at 1200°C. (a) NiAl+Hf, (b) NiAl-1Re+Hf, and (c) NiAl-2Cr+Hf.

Figure 15. EPMA back scattered electron image of a polished cross-section of NiAl-1Re+Hf after 10, 100h cycles at 1200°C. The bright particles are α-Re.

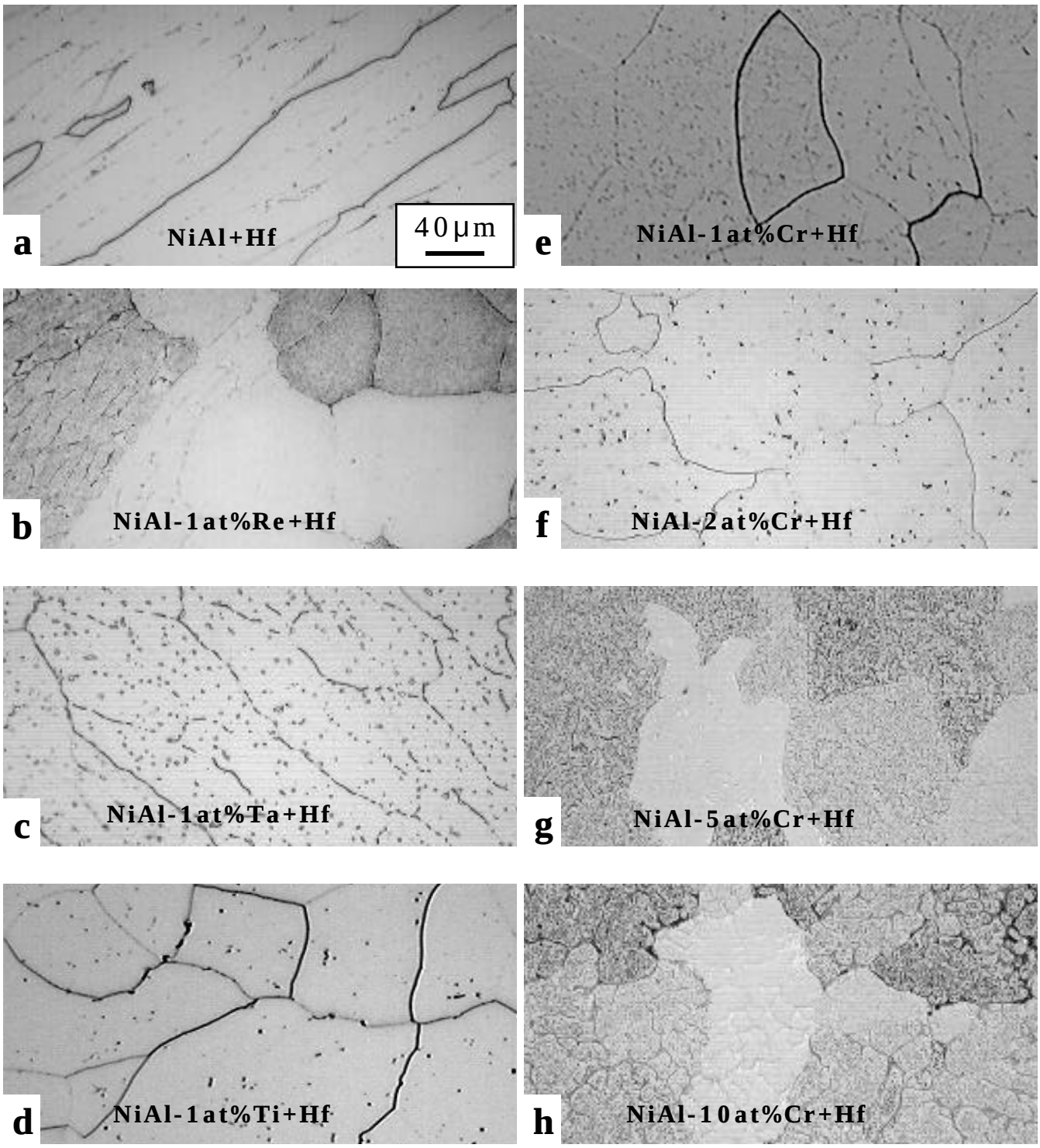

Figure 1. Metallographic analysis of the as-annealed alloys. (a) NiAl+Hf, (b) NiAl-1Re+Hf, (c) NiAl-1Ta+Hf, (d) NiAl-1Ti+Hf, (e) NiAl-1Cr+Hf, (f) NiAl-2Cr+Hf, (g) NiAl-5Cr+Hf and (h) NiAl-10Cr+Hf.

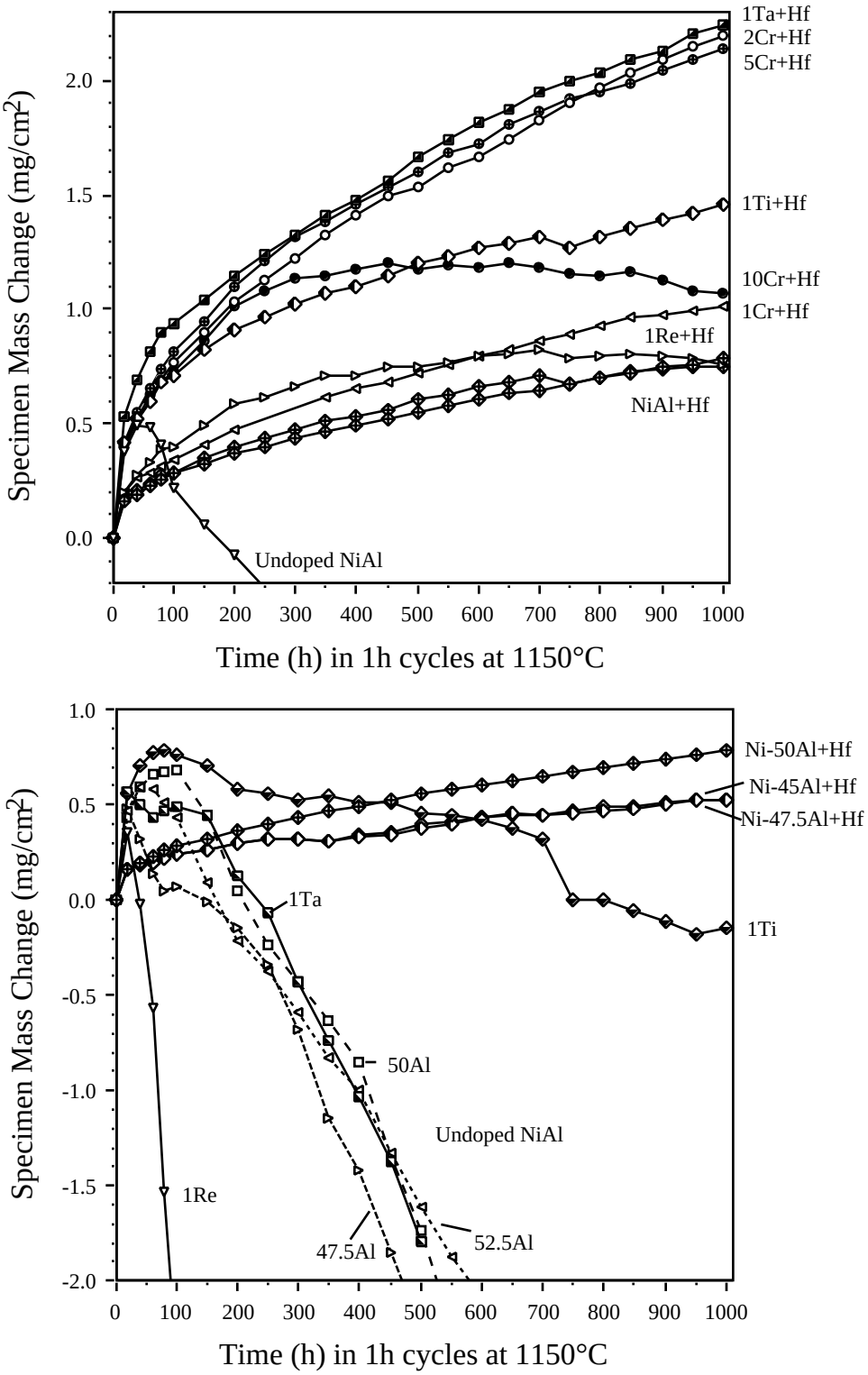

Figure 2. Specimen mass change for specimens tested in 1h cycles at 1150°C. Additions of Ta and Cr increased the mass gain by a factor of 4 compared to Hf-doped NiAl. Doping with Ti had a lesser effect and the downward trend of the Re-containing alloy indicates that it began to spall during the test.

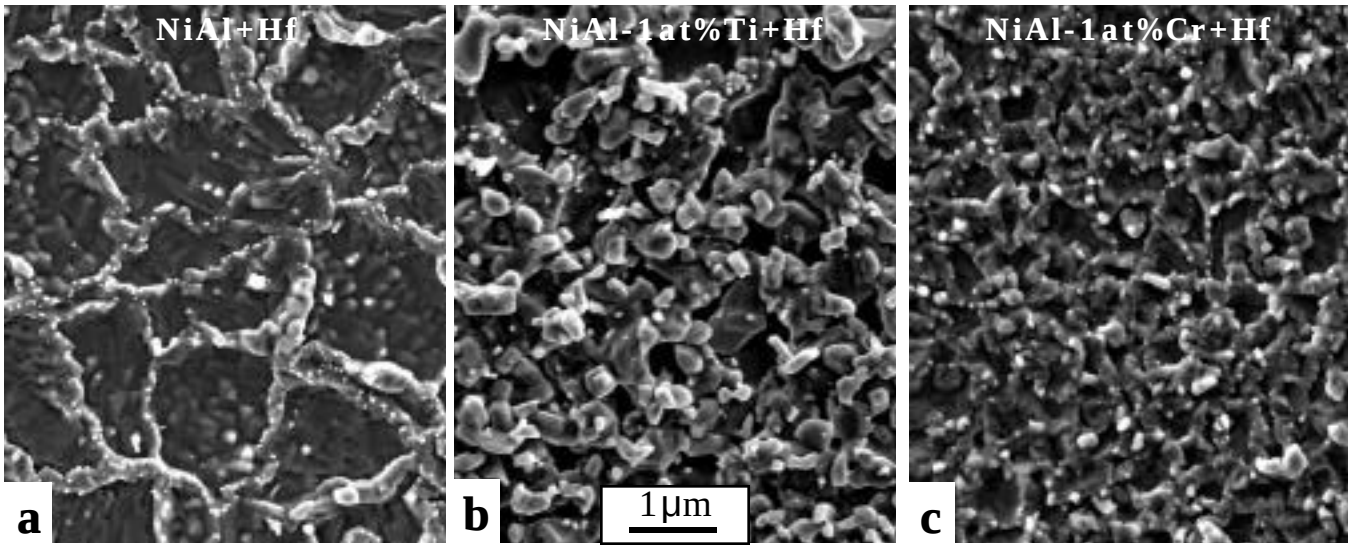

Figure 3. SEM plan view images of the surface scale after 1000x1h at 1150°C. (a) NiAl+Hf, (b) NiAl-1Ti+Hf and (c) NiAl-1Cr+Hf.

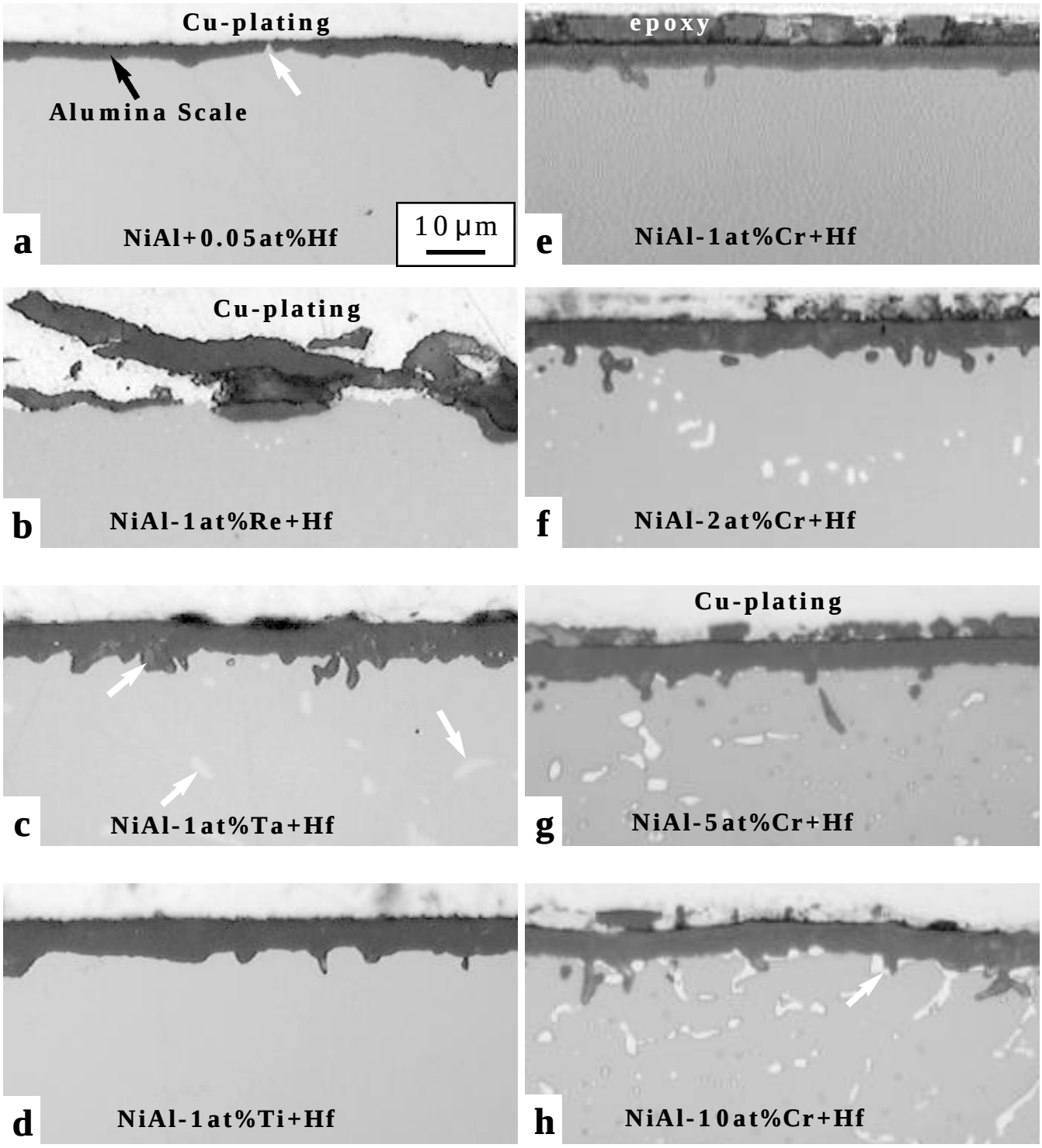

Figure 4. Metallographic cross-sections of the surface scale after 1000x1h at 1150°C. (a) NiAl+Hf, (b) NiAl-1Re+Hf, (c) NiAl-1Ta+Hf, (d) NiAl-1Ti+Hf, (e) NiAl-1Cr+Hf, (f) NiAl-2Cr+Hf, (g) NiAl-5Cr+Hf and (h) NiAl-10Cr+Hf.

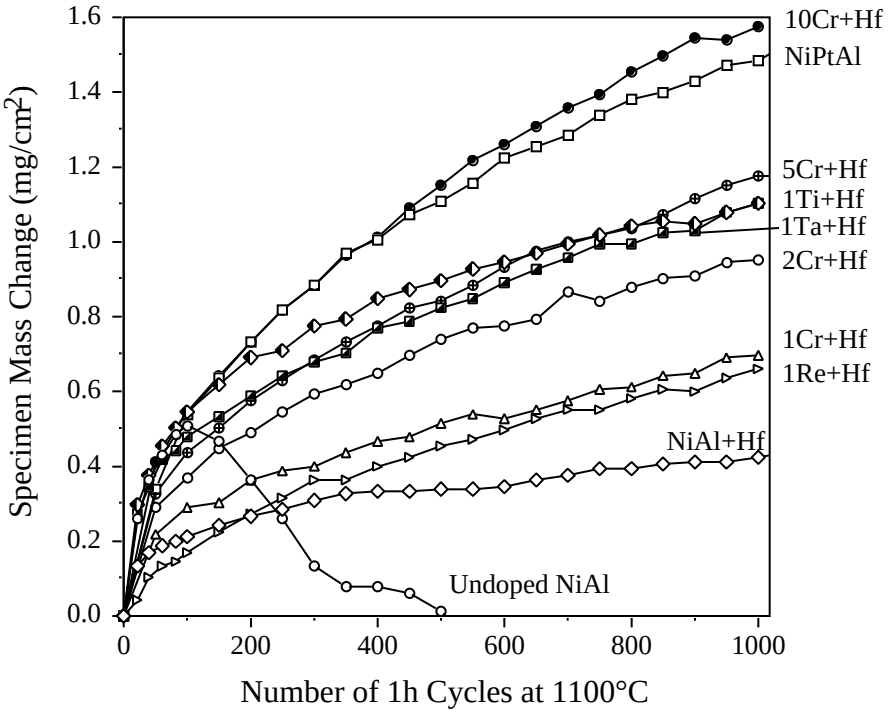

Figure 5. Specimen mass change for specimens tested in 1h cycles at 1100°C. Increasing amounts of Cr showed higher mass gains compared to the base NiAl+Hf material. A NiPtAl specimen was included to show the mass gain for an adherent, undoped alumina scale.

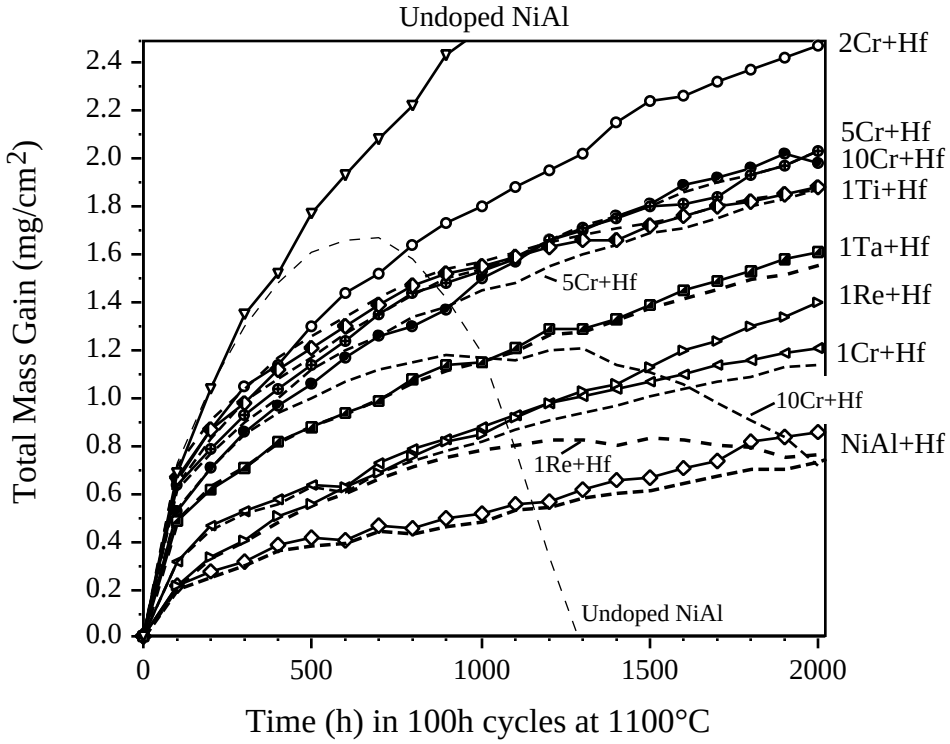

Figure 6. Total mass gain for specimens tested in 100h cycles at 1100°C are shown in sold lines with symbols while the dashed lines are the specimen mass changes. Separation between the two lines indicates the amount of scale spallation. A very low mass gain was observed for NiAl+Hf compared to the other alloy. The final data are summarized in Table III.

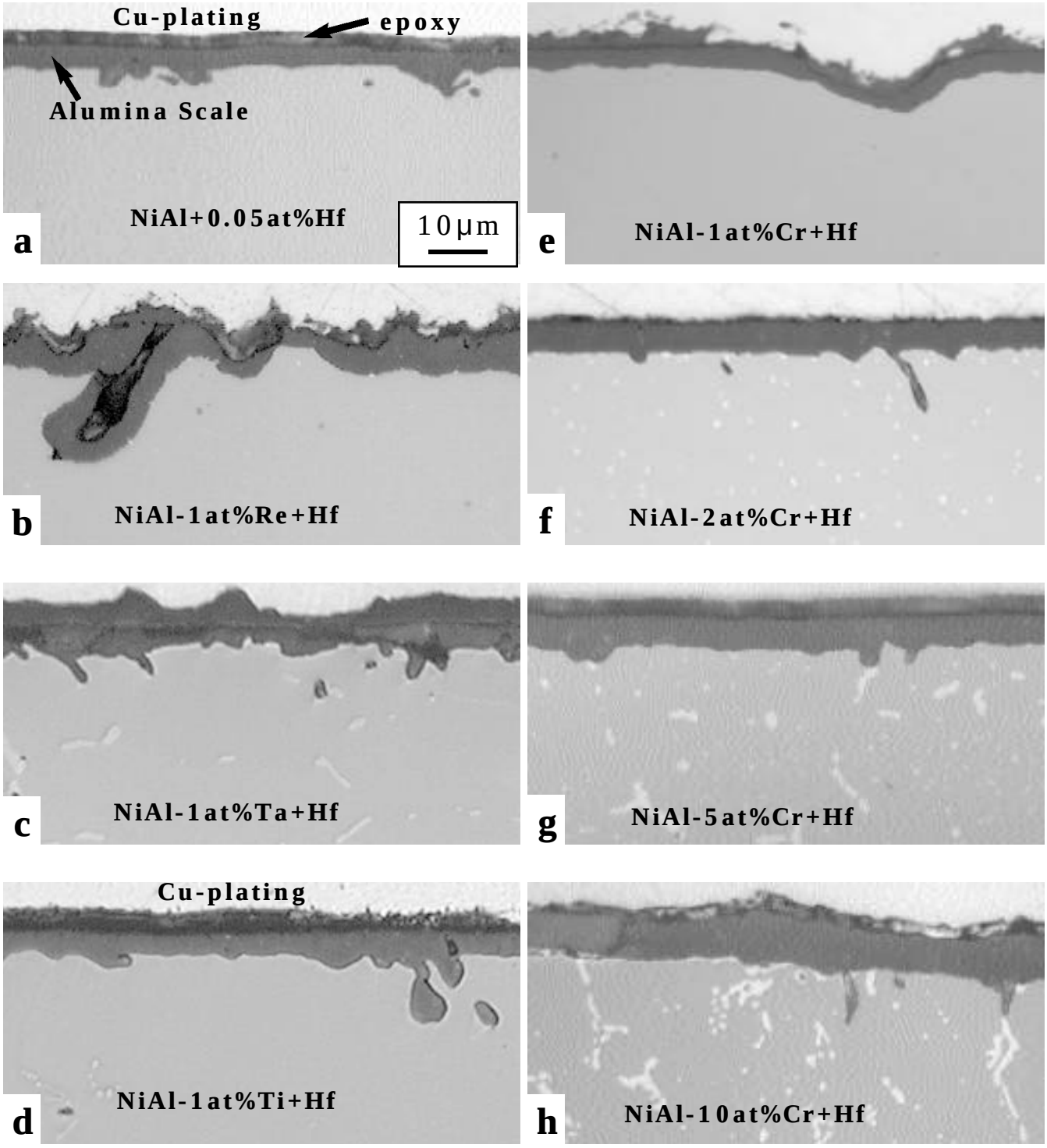

Figure 7. Metallographic cross-sections of surface scale after 20x100h at 1100°C. (a) NiAl+Hf, (b) NiAl-1Re+Hf, (c) NiAl-1Ta+Hf, (d) NiAl-1Ti+Hf, (e) NiAl-1Cr+Hf, (f) NiAl-2Cr+Hf, (g) NiAl-5Cr+Hf and (h) NiAl-10Cr+Hf.

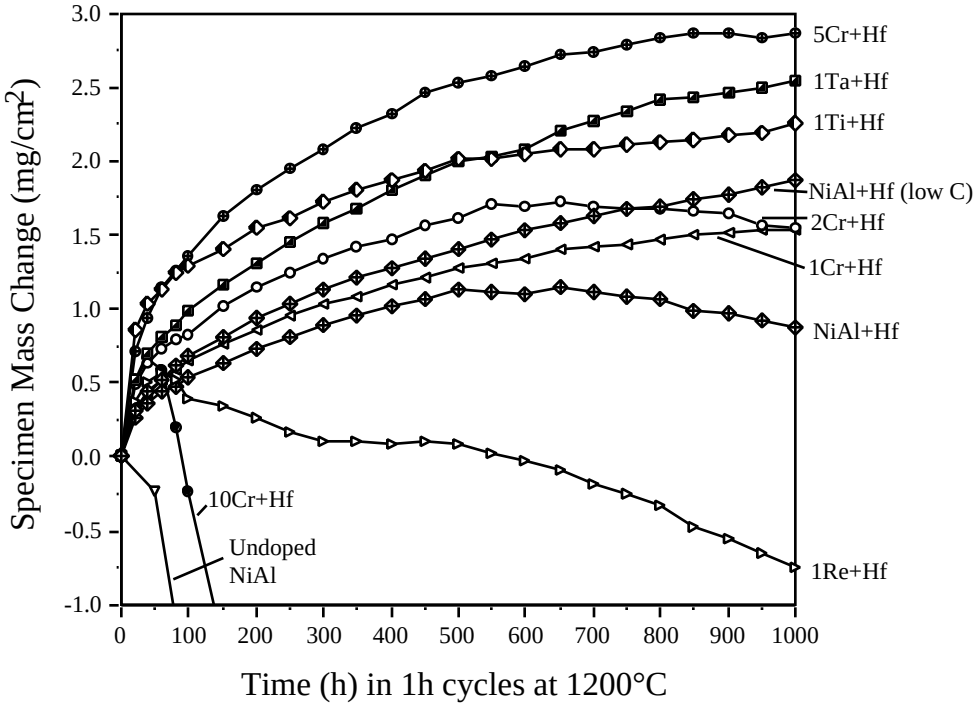

Figure 8. Total mass gain for specimens tested in 1h cycles at 1200°C. The high temperature and frequent cycling likely cause some degree of spallation in all cases. The addition of 5Cr significantly increased the amount of scale formed and the addition of Re increased the amount of spallation.

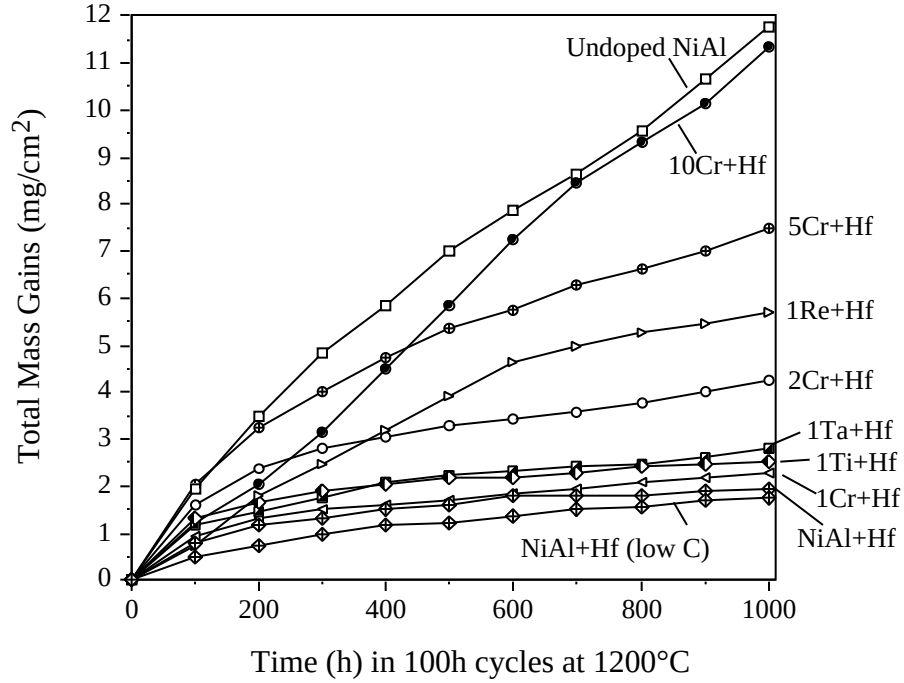

Figure 9. Total mass gain for specimens tested in 100h cycles at 1200°C. The low total mass gain for NiAl+Hf reflects the slow alumina growth rate and virtually no spallation. Higher mass gains with 1Cr, Ta and Ti reflect a faster scale growth rate. The other alloys have some degree of spallation, resulting in higher total mass gains. Undoped NiAl spalled almost all oxide after each cycle.

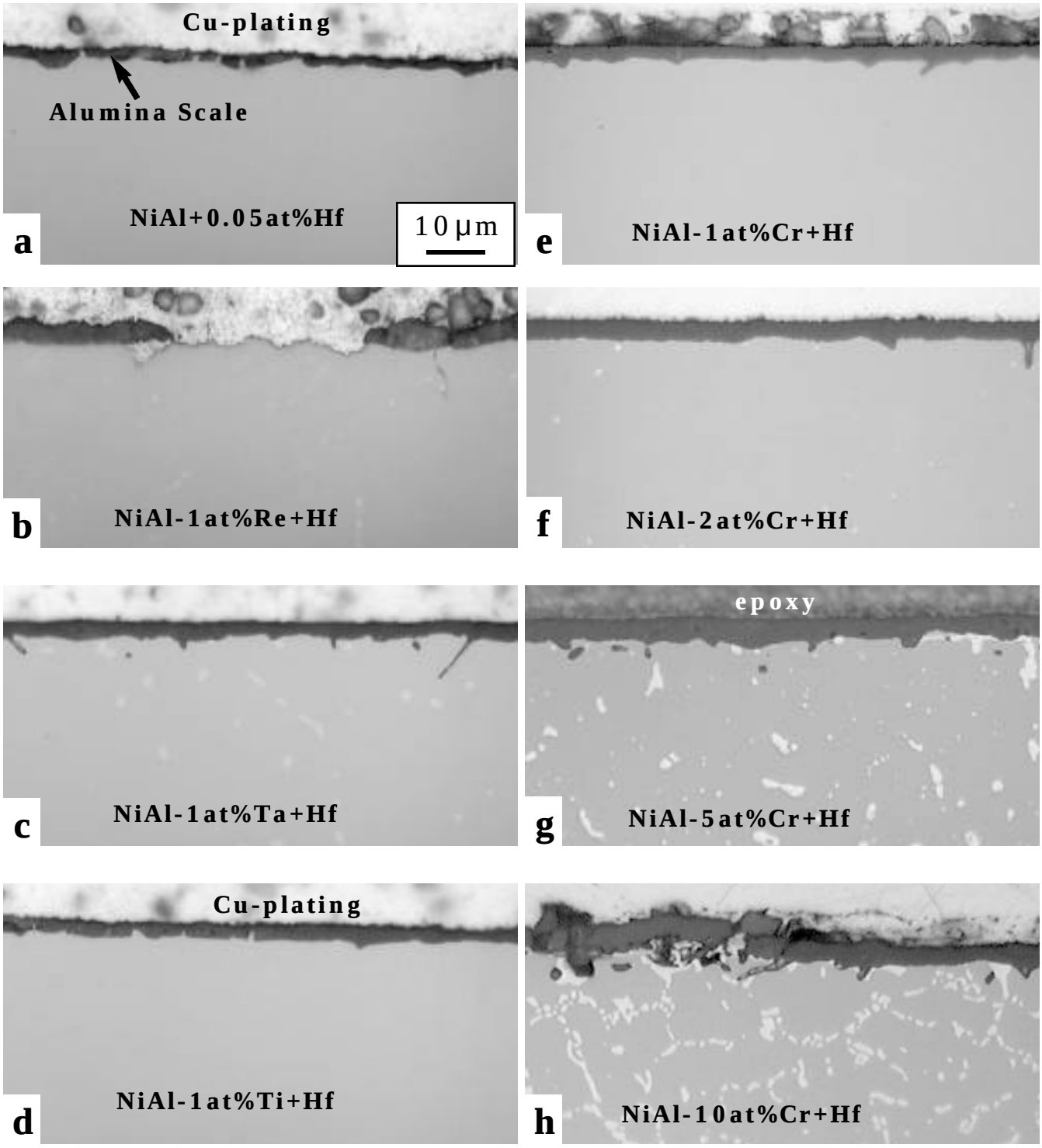

Figure 10. Metallographic cross-sections of surface scale after 100h at 1200°C. (a) NiAl+Hf, (b) NiAl-1Re+Hf, (c) NiAl-1Ta+Hf, (d) NiAl-1Ti+Hf, (e) NiAl-1Cr+Hf, (f) NiAl-2Cr+Hf, (g) NiAl-5Cr+Hf and (h) NiAl-10Cr+Hf.

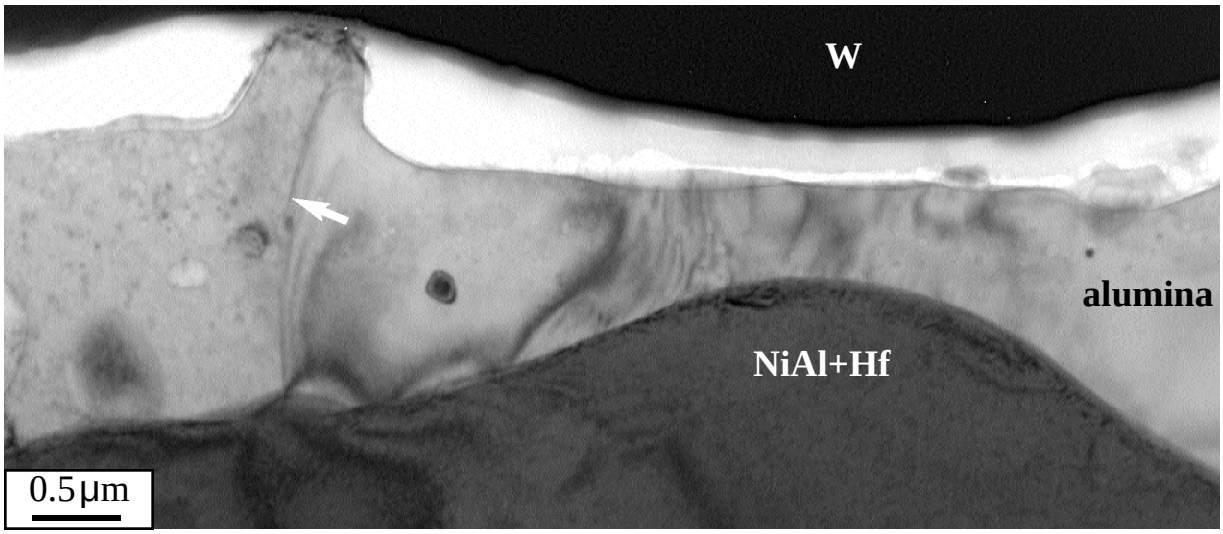

Figure 11. TEM bright field image of the alumina scale formed on NiAl+Hf after 2h at 1200°C. A grain boundary (arrow) was associated with the ridge at the gas interface and the scale is much thinner away from the grain boundary. A W layer was added during FIB specimen preparation layer to protect the gas interface of the scale.

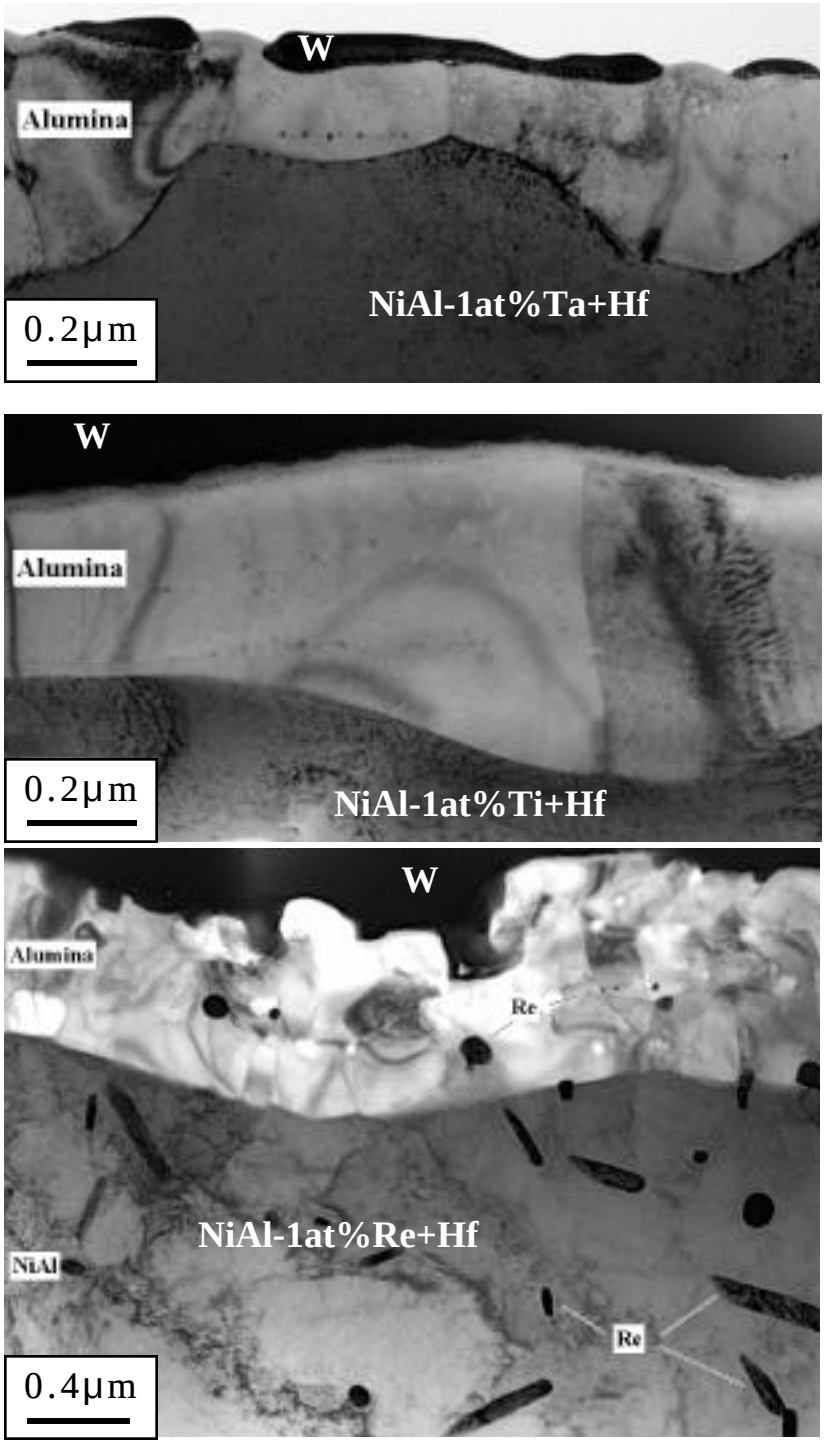

Figure 12. TEM bright field images of W-coated FIB-prepared scale cross-sections after 2h at 1200°C, (a) NiAl+1%Ta+0.05Hf, (b) NiAl+1%Ti+0.05Hf and (c) NiAl+1%Re+0.05Hf. The addition of Re (c) results in a more defective oxide with numerous voids and α-Re precipitates in the metal and in the scale.

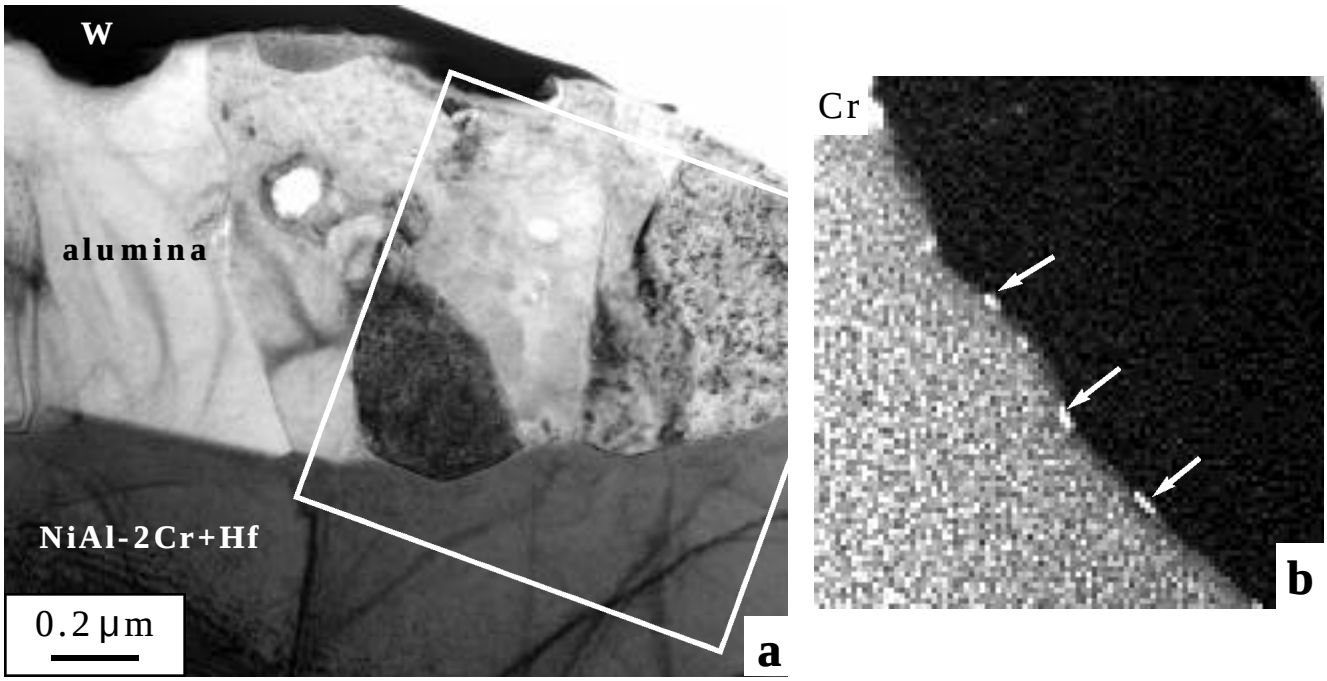

Figure 13. (a) TEM bright field image of the alumina scale formed on Ni-49Al-2Cr+Hf after 2h at 1200°C; (b) Cr EDS X-ray map at the interface reveals Cr-rich precipitates (arrows) in the metal adjacent to the metal-scale interface. A W layer was added during specimen preparation.

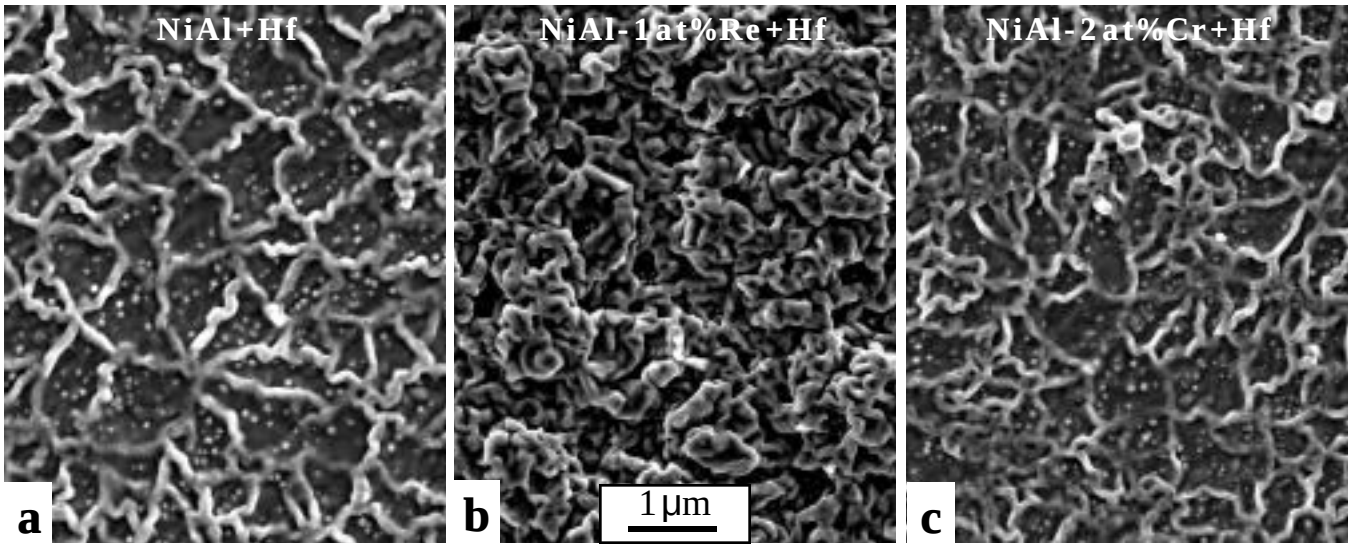

Figure 14. SEM plan view images of the surface scale after 2h at 1200°C. (a) NiAl+Hf, (b) NiAl-1Re+Hf, and (c) NiAl-2Cr+Hf.

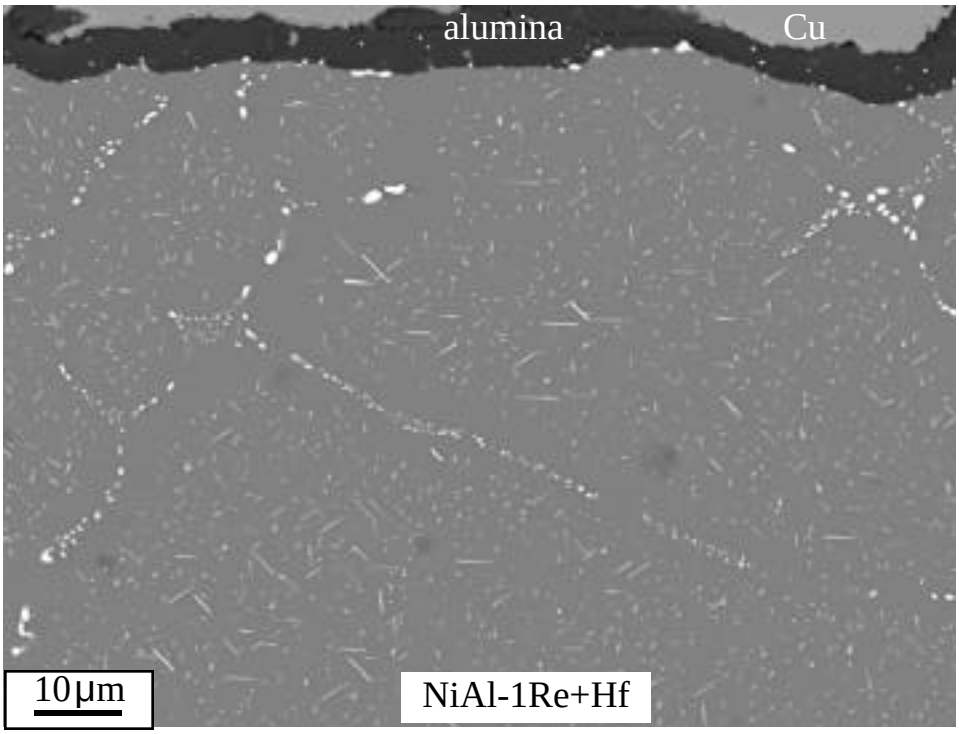

Figure 15. EPMA back scattered electron image of a polished cross-section of NiAl-1Re+Hf after 10, 100h cycles at 1200°C. The bright particles are α-Re.